Spectrochimica Acta Part A: Molecular and Biomolecular Spectroscopy 311 (2024) 124046



Contents lists available at ScienceDirect

Spectrochimica Acta Part A:
Molecular and Biomolecular Spectroscopy

journal homepage: www.journals.elsevier.com/spectrochimica-acta-part-a-molecular-and-biomolecular-spectroscopy





Surface-enhanced Raman spectroscopy of the filtrate portions of the blood serum samples of breast cancer patients obtained by using 30 kDa filtration device

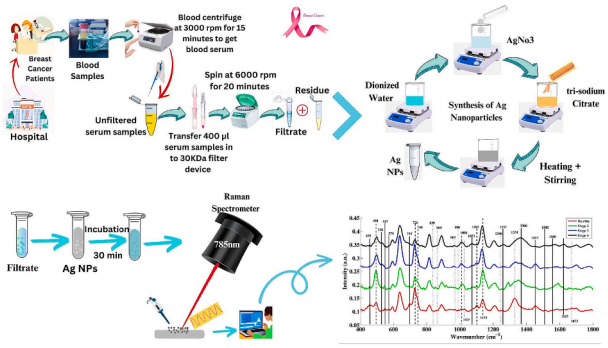
Hawa Hajab [a,1], Ayesha Anwar [a,1], Haq Nawaz [a,*], Muhammad Irfan Majeed [a,*], Najah Alwadie [b,*], Sana Shabbir [a], Arooj Amber [a], Muhammad Idrees Jilani [c], Hafiza Faiza Nargis [a], Muhammad Zohaib [d], Sidra Ismail [e], Abida Kamal [a], Muhammad Imran [f]

[a] Department of Chemistry, University of Agriculture Faisalabad, Faisalabad, Pakistan
[b] Department of Physics, College of Science, Princess Nourah bint Abdulrahman University, P.O. Box 84428, Riyadh 11671, Saudi Arabia
[c] Department of Chemistry, The University of Lahore, Lahore, Pakistan
[d] Department of Zoology, University of Agriculture Faisalabad, Faisalabad, Pakistan
[e] Medical College, Foundation University Islamabad, Pakistan
[f] Department of Chemistry, Faculty of Science, King Khalid University, P.O. Box 9004, Abha, Saudi Arabia

HIGHLIGHTS

- Surface enhanced Raman spectroscopy is employed to characterize the centrifuged serum samples of different stages breast cancer patients and healthy ones.
- In Surface Enhanced Raman Spectroscopy (SERS), silver nanoparticles function as substrates for amplifying signals.
- Some Surface Enhanced Raman Spectroscopy spectral features are associated with breast cancer samples in comparison with healthy ones which can be employed for diagnostic purpose.
- Principal components analysis (PCA) is found helpful for the differentiation between SERS spectral data of breast cancer and healthy samples.
- Partial Least discriminant Analysis (PLSDA) model is validated and can be used for the classification of breast cancer and healthy samples.

GRAPHICAL ABSTRACT



ARTICLE INFO

Keywords:
Breast cancer
Blood serum
Centrifugal filtration

ABSTRACT

Raman spectroscopy is reliable tool for analyzing and exploring early disease diagnosis related to body fluids, such as blood serum, which contain low molecular weight fraction (LMWF) and high molecular weight fraction (HMWF) proteins. The disease biomarkers consist of LMWF which are dominated by HMWF hence their analysis is difficult. In this study, in order to overcome this issue, centrifugal filter devices of 30 kDa were used to obtain

* Corresponding authors.
E-mail addresses: haqchemist@yahoo.com (H. Nawaz), irfan.majeed@uaf.edu.pk (M.I. Majeed), nhalwadie@pnu.edu.sa (N. Alwadie).
[1] First two authors have equal contribution.

https://doi.org/10.1016/j.saa.2024.124046
Received 4 December 2023; Received in revised form 4 February 2024; Accepted 12 February 2024
Available online 13 February 2024
1386-1425/© 2024 Elsevier B.V. All rights reserved.

Multivariate data analysis
Surface-enhanced Raman spectroscopy

filtrate and residue portions obtained from whole blood serum samples of control and breast cancer diagnosed patients. The filtrate portions obtained in this way are expected to contain the marker proteins of breast cancer of the size below this filter size. These may include prolactin, Microphage migration inhabitation factor (MIF), γ-Synuclein, BCSG1, Leptin, MUC1, RS/DJ-1 present in the centrifuged blood serum (filtrate portions) which are then analyzed by the SERS technique to recognize the SERS spectral characteristics associated with the progression of breast cancer in the samples of different stages as compared to the healthy ones. The key intention of this study is to achieve early-stage breast cancer diagnosis through the utilization of Surface Enhanced Raman Spectroscopy (SERS) after the centrifugation of healthy and breast cancer serum samples with Amicon ultra-filter devices of 30 kDa. The silver nanoparticles with high plasmon resonance are used as a substrate for SERS analysis. Principal Component Analysis (PCA) and Partial Least Discriminant Analysis (PLS-DA) models are utilized as spectral classification tools to assess and predict rapid, reliable, and non-destructive SERS-based analysis. Notably, they were particularly effective in distinguishing between different SERS spectral groups of the cancerous and non-cancerous samples. By comparing all these spectral data sets to each other PLSDA shows the 79 % accuracy, 76 % specificity, and 81 % sensitivity in samples with AUC value of AUC = 0.774 SERS has proven to be a valuable technique for the rapid identification of the SERS spectral features of blood serum and its filtrate fractions from both healthy individuals and those with breast cancer, aiding in disease diagnosis.

1. Introduction

Breast cancer (BC) is the most common malignancy occurring in the women with over 2 million cases identified in the recent year 2020 [1] accounting for 11.7 % total cases worldwide [2]. Breast cancer is identified as a molecularly heterogenous disease of neoplasm originating from the epithelial cells that line the mammary duct [3]. The incidence rate of breast cancer has been similar in developed and underdeveloped countries as in Latin America and Caribbean the frequently diagnosed disease among women is breast cancer. Detection of breast cancer patients at earlier stage substantially leads to less chances of mortality than those who are diagnosed at late-stage of breast cancer [4].

The techniques recommended by physician recently used to diagnose and subsequent treatment of malignancy and breast cancer include X-ray imaging, mammography, a core needle biopsies [5] magnetic resonance imaging (MRI), fluorescence, optical bioluminescence and optical imaging [6–8]. There is much increasing demand for a method that can easily and accurately detect early-stage symptoms without the need for labels, real time and with minimal invasiveness. These techniques demonstrate limited resolution and sensitivity, and their use can be detrimental to patients due to the potential harm from the ionizing radiation of X-rays during screening [8].

Biomarkers associated with various diseases can be identified in urine, blood, and serum samples [9] in this regards body fluids plays a crucial rule to facilitate efficient observation and rapid screening of cancer patients. They also help to find out specific biomarkers that indicate the presence of the disease [10]. To Identifying disease-specific biomarkers through the analysis of human serum poses significant challenges [11]. Human blood serum is characterized by its intricate composition, consisting of proteins, amino acids, lipids and carbohydrates [12]. Moreover, it contains a range of proteins, some of which exist in lower molecular weight fractions, while others, notably albumin, are present in substantial quantities within the high molecular weight fractions. While low molecular weight fractions (LMW) of proteins are regarded as potential disease biomarkers, the exploration of disease-specific biomarkers in the entire human serum poses challenges. This difficulty arises from the presence of high molecular weight proteins like albumin and globulin in blood serum, which actively inhibit the detection of low molecular weight proteins, thereby complicating their identification [13].

About 90 % of the entire protein composition in the serum is constituted by six proteins, each with a molecular weight exceeding 50 kDa. These Proteins are α1-Antitrypsin (52 kDa), Albumin (66 kDa), immunoglobulin G(IgG) with (150 kDa), transferrin (80 kDa), immunoglobulin A (IgA) 180–500 kDa and immunoglobulin M (IgM) (950 kDa) [14,15]. In the context of breast cancer, a significant array of biomarkers is evident across different stages. In this study 30 kDa centrifugal filter devices are employed because significant portion of breast cancer biomarkers and disease related proteins typically smaller than 30 kDa in size, of which more than five major proteins of different molecular weight are prolactin (12 kDa) [16], Microphage migration inhabitation factor (MIF)(12.5 kDa) [17], γ-Synuclein, BCSG1 (16 kDa) [18,19], Leptin (16 kDa) [20], MUC1 (17 kDa) [21], RS/DJ-1 (20 kDa) [22]. The proteins identified as potential biomarker targets are isolated through centrifugal filtration using a 30 kDa filter size. Consequently, serum samples are subjected to centrifugation employing devices with a kDa specification to distinguish between LMWF and HMWF. Subsequent to centrifugal filtration, Surface-enhanced Raman spectroscopy (SERS) was employed to analyze the spectral characteristics associated with different breast cancer biomarkers in the low molecular weight protein fractions (LMWF). After centrifugation through filter devices two fractions were obtained including HMWF and some LMWF. The latter comprises potentially disease-related proteins. Surface-Enhanced Raman Spectroscopy (SERS) is utilized to analyze low molecular weight proteins (LMW), identifying biochemical changes within distinct fractions in breast cancer patients and contrasting them with those in healthy individuals.

Raman spectroscopy is a valuable tool for biochemical analysis and provide insights in to molecular conformation and structure through a distinctive fingerprinting process [23,24]. Currently, Raman spectroscopy, along with Surface-enhanced Raman spectroscopy, has proven valuable in diagnosing various diseases, including dengue [25] hepatitis C [26] almost all types of cancer especially breast cancer [27] prostate cancer [28] cervical cancer [29] and tuberculosis [30]. SERS is a versatile technique that significantly improves diagnostic accuracy and is a reliable, cost effective procedure that requires less time and a small amount of sample making it an excellent choice for sample identification [31]. Due to their strong Plasmon resonance silver and gold nanoparticles are used as SERS substrate. Silver nanoparticles has been extensively employed as an efficient substrate and its mostly used for different microbial analysis in multiple previous studies [32,33]. Surface-enhanced Raman spectroscopy (SERS) has also been utilized for the discrimination of healthy individuals and diagnosed breast cancer serum samples for the identification of highly specific disease-related biomarkers in human blood serum, following centrifugation with filtration devices of specific sizes in kDa [34].

In this study, blood serum samples of the breast cancer patients are filtered using 30 kDa filter devices in order to get the filtrate portions of these samples to target the marker proteins of the size below 30 kDa

including prolactin, Microphage migration inhabitation factor (MIF), γ-Synuclein, BCSG1, Leptin, MUC1, RS/DJ-1 These centrifuged samples are further analyzed by the SERS technique to identify the SERS spectral features related to development of breast cancer in the samples of different stages as compared to the healthy ones. The primary aim of this study is to achieve early-stage breast cancer diagnosis through the utilization of Surface-enhanced Raman spectroscopy (SERS) after the centrifugation of serum samples with Amicon ultra-filter devices of 30 kDa. According to the best of our knowledge, there is no such report published yet.

2. Materials and methods

2.1. Sample preparation and protocol

Breast cancer serum samples were collected from Allied Hospital and PINUM hospital Faisalabad, including 10 healthy controls and 26 samples from different stages of breast cancer. Notably, the available stages are stage, 2, stage 3 and 4. The samples collected in this study were exclusively from females, specifically within the age range of 50 to 55 years old. A summary of the ages of all the patients for this study are mentioned in Table 1. Samples from stage-1 were unavailable for analysis due to infrequent presentation of patients at this particular disease stage within the clinical setting. These samples were collected at the early morning from patients after overnight fasting. The blood samples were centrifuged at 3000 rpm for 15 min to obtain blood serum. Blood serum was further centrifuged by using 30 kDa filter devices, Amicon ultra 2 ml (Merck Millipore) to obtain filtrate portions of these samples to target the proteins biomarker. For centrifugal filtration 400ul serum was transferred into device and spun at 6000 rpm for 20 min. After centrifugation two fractions are obtained, one is HMW fraction called residue/concentrate and the other is LMW fraction called filtrate fraction. This protocol is followed from the literature [35]. A summary of the samples collected for this study is provided in the Supplementary material in Table 1.

2.2. Preparation of silver nano particles

Silver nanoparticles (Ag-NPs), employed as SERS measurement substrates, were synthesized through a chemical reduction method. In the synthesis of Ag-NPs, silver nitrate ($AgNO_3$) served as the precursor, and trisodium citrate ($Na_3C_6H_5O_7$) functioned as both the reducing and capping agent. More briefly to prepare 1 mM solution, 33.72 mg of $AgNO_3$ were added to the beaker containing 200 ml deionized water which was heated until it started boiling, after this addition of 8 ml of 1 % $Na_3C_6H_5O_7$ and heated again until one and half hour with continuous stirring of 600 rpm. Following this step, the solution was allowed to cool at room temperature, resulting in the formation of gray-colored Ag-NPs. These nanoparticles exhibited an oval shape geometry with a diameter of 65×45 nm, as detailed in our prior study [26].

2.3. SERS spectral acquisition

For SERS spectral measurements, the filtrate samples of different stages along with the healthy ones are used which are obtained after the centrifugation of serum samples with Amicon ultra-filter devices of 30 kDa. Afterward 40 μl sample of filtrate fractions mixes with 40 μl of nanoparticles followed by incubation time of 30 min which allowed nanoparticles to interact with samples effectively. From this incubation mixture, a 40 μl sample was placed onto an aluminum slide. Spectral acquisition was performed using the Raman microscope ATR8300BS Optosky, China, with the laser power focused on each sample through a 40X objective lens, capturing 15 spectra for each sample. For this purpose, 50 mW laser power was employed with a 10-second integration time, and the SERS spectra were recorded within the range of 400 to 1800 cm^{-1}. SERS data acquisition conditions were kept the same for all filtrate samples.

Table 1
Distinctive breast cancer biomarkers in the size range of the 30 kDa filter.

Breast cancer biomarkers	Molecular weight	References
Prolactin	12 kDa	[16]
Microphage migration inhabitation factor (MIF)	12.5 kDa	[17]
γ-Synuclein, BCSG1	16 kDa	[18,19]
Leptin	16 kDa	[20]
MUC1	17 kDa	[21]
RS/DJ-1	20 kDa	[22]

2.4. SERS data pre-processing

The preprocessing of SERS spectral data was performed in the MATLAB 7.8 version with established protocols. The raw spectral data was pre-processed and unwanted components like noise, baseline correction and substrate subtraction were performed prior to the spectral analysis [36]. Baseline was corrected by employing rubber band and polynomial algorithm (13point order). The normalization of the spectra was performed by vector normalization and smoothing by Savitzky-Golay smoothing method of (3, 15 point window command) [37].

2.5. SERS data analysis

The processed data in this study were analyzed by variety of multivariate data analysis approaches such as Principal Components Analysis (PCA) and Partial Least Square Discriminant Analysis (PLS-DA). The aim was to investigate the notable variations within datasets representing both control groups and different stages of breast cancer. PCA, an unsupervised statistical technique, simplifies interconnected variables into a more condensed set of independent variables referred to as principal components (PCs). These principal components contribute to simplifying the data's complexity while retaining its essential variability. The most significant source of variations is explained by the PC-1 and subsequent variability in the spectral datasets is explained by PC-2 and so on. The PC loadings represent distinct dimensions and variations that are isolated and plotted. This helps in observing the features variances contributing to differences in SERS spectral data. [37]. PCA loadings plots show influence of SERS bands in data clustering indicating strong co-relation with specific PC's which provide insight about variation among samples [38].

PLS-DA, a predictive modeling method, holds the capability to categorize, elucidate, and differentiate variability within datasets by analyzing their spectral patterns and class information. It integrates two approaches—Partial Least Square (PLS) and Linear Discriminant Analysis [39].

The PLS-DA model is constructed based on X and Y variables, which represent SERS spectral data and details about different spectral data classes. SERS data for each sample is sourced from a single variable in the MATLAB workspace. Afterward, various variables from each sample are structured into a matrix using a specific arrangement. To ensure impartial results, the spectral data is randomized. The dataset is divided, with 60 % designated for training and 40 % for validation. The model is fine-tuned on the spectral datasets using the Bayes algorithm with leave-one-sample-out cross-validation (LOOCV), where each of the 15 spectra is successively excluded during the validation process.

The Receiver Operating Characteristic curve (ROC) is commonly employed to assess the diagnostic accuracy and evaluate the performance of binary classifier models, serving as a measure of the technique's utility. In binary classification a graphical representation is generated, illustrating the relationship between true positive (indicating sensitivity) and a false positive rates (indicating specificity), respectively [40].

3. Results and discussion

3.1. Mean SERS spectra of centrifuged versus uncentrifuged/whole healthy serum samples

The comparison between mean SERS spectra acquired from the centrifuged healthy sample (residue and filtrate portions) and uncentrifuged healthy whole serum sample were is in Fig. 1 and their peaks assignment are described in Table 2 along with references.

The mean SERS spectra of healthy whole serum, residue and filtrate portions are shown in Fig. 1 which clearly indicate the SERS spectral features are prominent in filtrate portion. SERS bands which are only present in filtrate portion (LMWF) are indicated by dotted lines. A medium intensity peak of 547 cm^{-1} (cholesterol in lipids) present in healthy portion.970 cm^{-1} (lipids), 990 cm^{-1} (Phosphorylation of proteins), 1008 cm^{-1} is assigned to (phenylaniline, protein), 1331 cm^{-1} (proteins). The SERS spectral characteristics indicated by dashed lines are consistently found in all serum samples from healthy/control, residue/concentrate and filtrate portion but with different intensities. A prominent peak present at 700 cm^{-1} which has medium intensity and slightly move forward in filtrate portion is due to the cholesterol(ester). The medium intensity peaks present in serum and residue portion and with very low intensity in filtrate is due to the amino acids, 1102 cm^{-1} (carbohydrates), the intense peak present at both centrifuged and uncentrifuged samples portion at 1133 cm^{-1} (palmitic acid) (fatty acids). Palmitic Acid demonstrates diverse pharmacological effects, encompassing antiviral, anti-inflammatory, analgesic properties, and the regulation of lipid metabolism [41,42]. Due to its anticancer attributes, studies have revealed that Palmitic Acid induces the halting of the cell cycle and facilitates programmed cell death in human neuroblastoma and breast cancer cells [43,44].

The indication of solid lines represents peaks present either in the residue and serum only or present in all. These peaks are 458, 476, 515, 749, 784, 962, 1024, 1073, 1181, 1293, 1453 and 1513 cm^{-1}. The peak is present at 458 cm^{-1} due to tryptophan (protein), 476 cm^{-1} (glutamate vibrations), 515 cm^{-1} (Phosphatidylinositol). A prominent SERS peak present at 749 cm^{-1} Thymine (ring breathing mode of DNA), 784 cm^{-1} (O-P-O Stretching), Peak at 962 cm^{-1} ($CH'_{2,6}$ bending protein), 1024 cm^{-1} (adenine). 1073 cm^{-1} (Triglycerides, fatty acids), 1181 cm^{-1} and 1293 cm^{-1} (C–H bending), 1453 cm^{-1} (amide II), 1513 cm^{-1} C═C stretching (carotenoids) beta-carotene. After analysis, it was observed that cancerous samples contain less concentrations of carotenoid as compared to the non-cancerous samples [45].

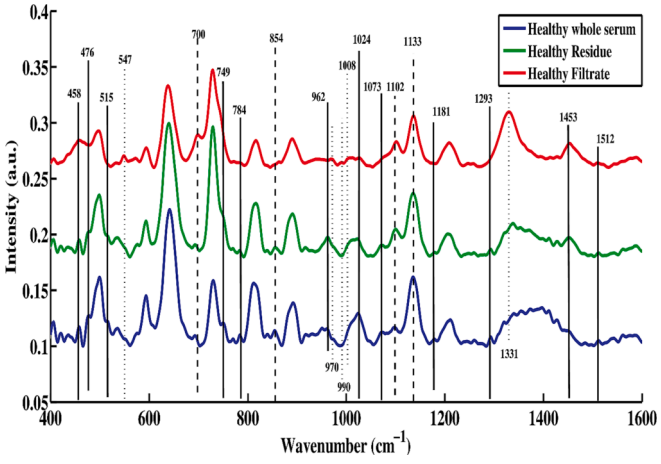


Fig. 1. Comparison of mean SERS spectra of filtrate fraction, residue, and whole serum samples of healthy control sample.

Table 2
SERS peak assignments of spectral features of filtrate fractions obtained by 30 kDa device of the healthy control and breast cancer stages.

Peaks Positions cm^{-1}	Peak Assignments	References
458	Protein, tryptophan (Ring torsion)	[47]
476	Glutamate (protein)	[47]
498	Tryptophan (protein)	[34]
515	Phosphatidylinositol (lipids)	[48]
528	Cholesterol, (vibrational modes)	[49]
547	Cholesterol (Lipids)	[50]
554	Carbohydrates	[51]
574	Tryptophan, Guanine (Ring breathing)	[2,52]
700	Cholesterol, (lipids)	[50]
728	Adenine ring (breathing mode)	[53,54]
744	Thymine (ring breathing mode in DNA)	[55]
749	Thymine (ring breathing)	[56]
784	DNA backbone (O–P–O Stretching)	[57]
839	α-Saccharide, (Carbohydrates)	[50]
854	Amino acid	[58]
864	C–H bond (bending vibration)	[59]
962	Protein ($CH'_{2,6}$ bending)	[60]
970	Vibration of ribose (protein)	[61]
990	Phosphorylation of proteins	[62,63]
1008	Phenylalanine, (protein)	[56,64,65]
1024	C–H deformation, Adenine, glycogen	[66,67]
1073	Triglycerides (Breast cancer), Fatty acids	[68,69]
1102	Carbohydrates	[70]
1133	Palmitic acid	[60,50]
1181	C–H bending mode, In plane ring distortion,	[56,71]
1246	Amide III	[52,72]
1257	lipids (═C–H in plane bending)	[73,26]
1293	C-H bending	[74]
1331	Proteins, nucleic acid bases	[75,76,77]
1366	Tryptophan	[78]
1453	Protein, (CH_2 bending mode in malignant tissues)	[79,80]
1508	Amide II, fibrinogen	[81,82,83]
1512	Carotenoids (In phase C═C stretching)	[84]
1560	Tyrosine, amide II (protein)	[58,85,86]
1588	C═CC Stretching mode in Adenine	[87]
1625	Amide I, protein	[88,89,90]
1673	Amide I	[91]

3.2. Mean SERS spectra of the filtrate portions of the blood serum samples of healthy and different breast cancer stages

All the SERS spectra collected from the filtrate portions of the healthy control (red) and breast cancer stages including stage 2 (green), stage3 (blue), stage 4 (black) are shown in Fig. 2. The solid lines distinguish between peaks found in healthy individuals and those in different breast cancer stages. These spectral features include 528, 574, 1073, 1257, 1366, 1508, 1560 and 1625 cm^{-1} which are only present in breast cancer stages easily differentiating them from healthy control samples hence may be considered as disease biomarkers. The less intense peak appears at 528 cm^{-1} (cholesterol and cholesteryl esters), 574 cm^{-1} (Tryptophan, protein), 1073 cm^{-1} in all stages due to the Triglycerides in (Breast cancer, Fatty acids), 1257 cm^{-1} is (═C–H in plane bending due to lipids), 1366 cm^{-1} (tryptophan, protein), 1560 cm^{-1} (amide II), 1625 cm^{-1} (Amide I,). Moreover, other solid line peaks of SERS spectral features are present at 458, 547, 700, 1453 and 1508 cm^{-1}, which are present in healthy as well as in breast cancer stages. At 458 cm^{-1} (tryptophan ring torsion), 547 and 700 cm^{-1} (Cholesterol), 1453 cm^{-1} (amide II) CH_2 bending mode in malignant tissues.1508 cm^{-1} may be caused by (Amide II) or fibrinogen and the prominent peak is observed in the filtrate portion of various stages of breast cancer but is absent in healthy filtrate samples. Here fibrinogen is important signaling molecule present in breast cancer tissues which leads to structural changes and conformation including glycol proteins. Hence the level of fibrinogen in breast cancer normally increases due to tumor inflammation and its progression in cells. However elevated level of fibrinogen may cause

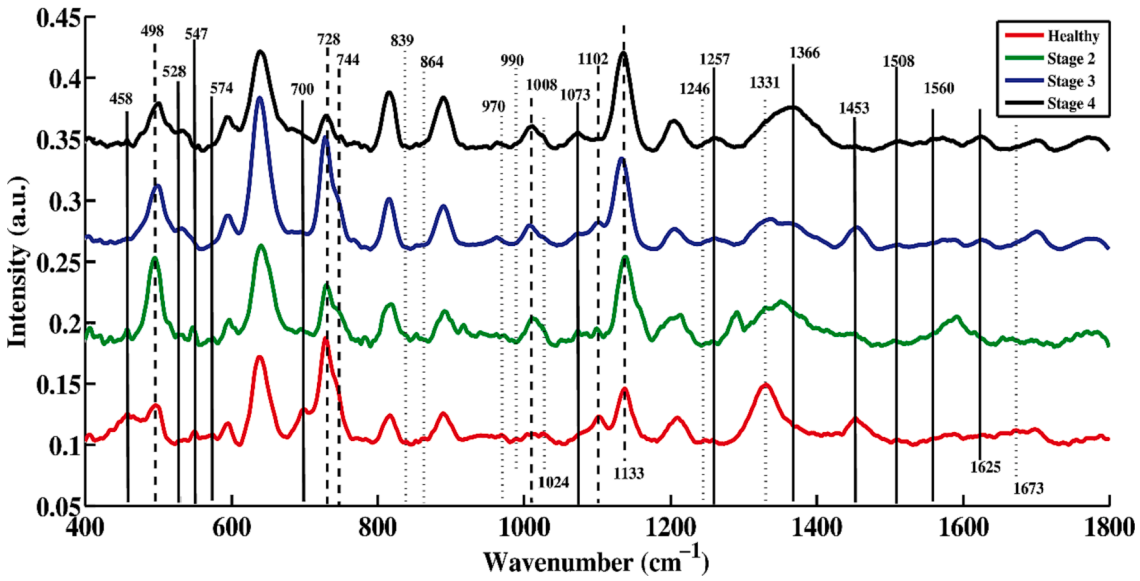


Fig. 2. Comparison of Mean SERS spectra of filtrate fractions of healthy and different stages of breast cancer patients.

several effects in lymph nodes which includes promoting the tumor, increasing the risk level of blood clotting which may potentially causes treatment outcomes [46].

The dashed lines indicated in the spectrum are labeled for the peaks having the intensity-based changes and these peaks are present both in the breast cancer and non-cancerous (healthy/control) samples. The peaks appearing at 498, 1008 and 1133 cm^{-1} have low intensity in non-cancerous samples as compared to the cancerous samples. The peaks appear at 498 cm^{-1} (tryptophan), 1008 cm^{-1} (phenylaniline), 1133 cm^{-1} (palmitic acids). The SERS feature at position 744 cm^{-1} (thymine) appears as a shoulder in healthy samples and then increase in intensity and becomes a clear peak at stage 4. Moreover, SERS band at 728 and 1102 cm^{-1} have medium intensities in the non-cancerous samples and of low intensities in the cancerous samples. The peak at 728 cm^{-1} (ring breathing mode in Adenine), 1102 cm^{-1} (carbohydrates). Preprocessed spectra of healthy and breast cancer disease samples are shown in Figs. S1–S4.

The dotted lines peaks are only present in only healthy control samples and not in any stage of cancer. 839 cm^{-1} α-saccharide (Carbohydrates), 864 cm^{-1} (bending vibration of C–H bond), 970 cm^{-1} (lipids), 990 cm^{-1} (Phosphorylation of proteins), 1024 cm^{-1} (Carbohydrates), 1246 cm^{-1} (Amide III), 1331 (Proteins) cm^{-1} and 1673 cm^{-1} (amide I). Comparison of Mean SERS spectra of filtrate fractions of healthy and different stages of breast cancer patients with standard deviation is presented in Fig. S5.

3.3. Principal components analysis (PCA)

The SERS spectra of all the low molecular weight fractions of healthy controls and breast cancer positive samples of different stages were

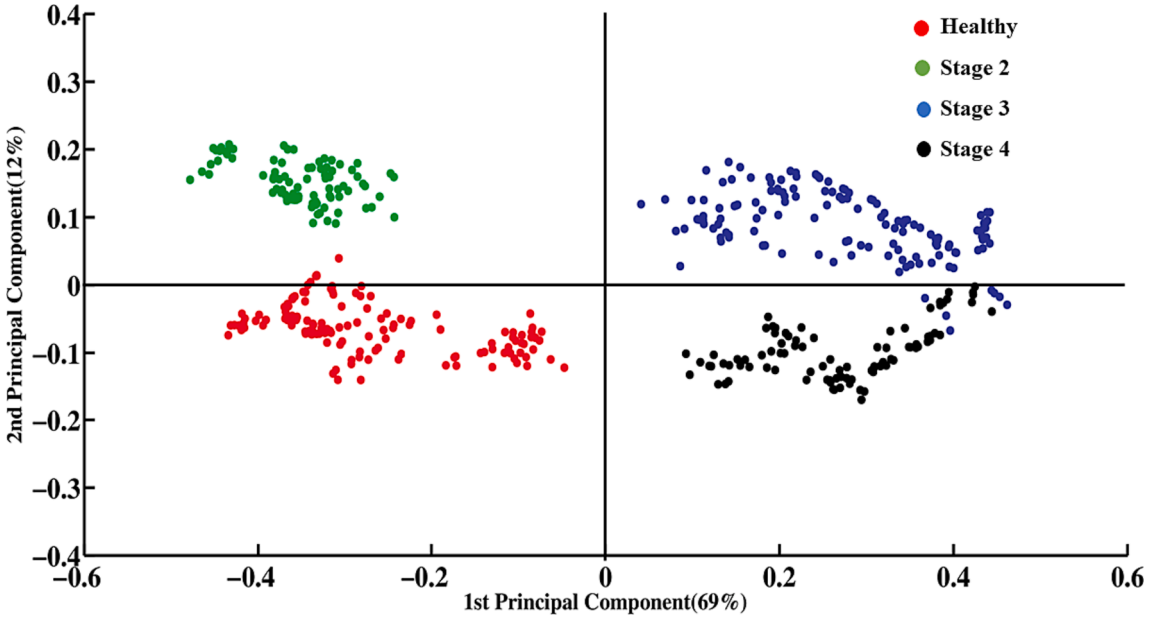


Fig. 3. PCA scatter plot of the SERS spectra of filtrate fractions of the blood serum samples of the healthy, stage 2, stage 3 and stage 4 breast cancer stages.

examined by PCA to differentiate and identify the characteristic SERS spectral features. Fig. 3 depicts the overall PCA scatter plot of all samples showing differentiation among them. Here SERS spectral data of the healthy samples (red clusters), stage2 (green), stage3 (blue) and stage 4 (black) are observed as separate clusters. Moreover, the red and green dots represent spectra of Healthy/controls and stage 2 and these are clustered on negative axis of PC1 while other clusters like blue and black dots represents spectral data sets of stage3 and stage clusters are on positive axis of PC1. The PC1 shows 69 % variability while PC2 shows 12 % variability in SERS spectra. Percentages of PCA algorithms is presented in Table 2.

Fig. 4a shows the pairwise PCA scatter plot and loadings of various breast cancer stages. Green color dots represent stage 2 which are clustered along negative axis of PC1, and blue color dots correspond to stage 3, clustered along positive axis of PC1. PCA clearly separates the samples from stages 2 and 3 and their variability in SERS spectra by PC1 is 61 % and PC2 is 8 %. Notably, Fig. 4b shows the PCA loading of these two stages where stage 2 associated with the negative loadings while stage 3 aligns to the positive loadings which are based on the clustering of these stages in scatter plot shown in Fig. 4a. The peaks in positive loadings are at 458 cm^{-1} (tryptophan), 476 cm^{-1} (glutamate, protein), 696 cm^{-1}, (amino acids), 728 cm^{-1} (adenine), 744 cm^{-1} (thymine), 854 cm^{-1} (amino acids), 962 cm^{-1} (Protein, $CH'_{2,6}$ bending) 1102 cm^{-1} (carbohydrates) and related to SERS spectral data of stage 3 breast cancer samples. While the peaks in negative loadings correspond to SERS spectral features of stage 2 are 498 cm^{-1} (tryptophan), 528 cm^{-1} (cholesterol vibrational mode), 547 cm^{-1} (cholesterol in lipids), 1133 cm^{-1} (palmitic acid), 1257 cm^{-1} (=C–H in plane bending, lipid) 1508 cm^{-1} (Amide II, fibrinogen). PCA average spectra scatter plot presented in Fig. S6.

Fig. 5a A pairwise PCA scatter plot illustrates the comparison between the filtrate portions of breast cancer serum from stages 2 and 4. PC1 accounts for 65 % of the differentiation, while PC2 contributes 18 %. In PC1, the positive axis clusters correspond to the SERS spectral features of stage 4. Hence, the stage 4 belongs to positive loadings shown in Fig. 5b and stage 2 clusters are on negative sides which are in green dots corresponds to the negative loadings in PC1. Moreover, Negative side clusters associated to the negative loadings and positive sides clusters illustrates the positive loadings in breast cancer samples. The SERS spectral features of stage 4 correspond to the positive axis in clusters in PC 1. Hence stage 4 belongs to positive loadings shown in Fig. 5b. The peaks appear at positive side have higher intensities. the peaks at 458 and 574 cm^{-1} (tryptophan), 728 cm^{-1} (Adenine ring breathing mode), 744 cm^{-1} (thymine), 1331 cm^{-1} (proteins), 1453 cm^{-1} (CH_2 bending) protein in malignant tissues, 1560 cm^{-1} (amide II), while in negative loading of stage 2 corresponds to the peaks 498 cm^{-1} (tryptophan), 528 cm^{-1} (cholesterol, vibrational mode), 1133 cm^{-1} (Palmitic acid), 1257 cm^{-1} lipids (=C–H in plane bending), 1366 cm^{-1} (tryptophan), 1508 cm^{-1} (amide II, fibrinogen), 1625 cm^{-1} (Amide I protein) as a results the presence of these peaks in stage 4 with higher intensities and in positive loading shows that enhancement of disease biomarkers in serum of advanced breast cancer stage 4 contrasted to stage 2.

In Fig. 6a pairwise PCA scatter plot are shown between stage 3 and stage 4 where dots representing stage 4 are clustered along positive axis of PC 2 and dots clustered along negative axis of PC 2 represents stage 3. The differentiation values explained by PC1 is 59 % and by PC2 17 % which distinctly shows the higher concentrations of disease biomarkers in these breast cancer stages. Fig. 6b shows PCA loadings in which positive loadings correspond to stage 4 and negative loadings correspond to stage 3. The positive loading peaks include 498 cm^{-1} (protein), 554 cm^{-1} (carbohydrates), 1008 cm^{-1} (phenylaniline, protein), 1133 cm^{-1} (Palmitic acid), 1257 cm^{-1} (=C–H in plane bending) lipids, 1508 cm^{-1} (amide II, fibrinogen), 1625 cm^{-1} (Amide I, protein) and stage 3 peaks corresponds to negative loadings peaks which includes 458 cm^{-1} (Protein, tryptophan (Ring torsion), 547 cm^{-1} (lipids, cholesterol), 728 cm^{-1} (Adenine ring breathing mode), 744 cm^{-1} (Thymine (ring breathing), 962 cm^{-1} (Protein $CH'_{2,6}$ bending), 1102 cm^{-1} (carbohydrates), 1453 cm^{-1} (Protein, malignant tissues (CH_2 bending).

The Fig. 7 shows the PCA loading plot of healthy control and breast cancer stages of filtrate portions which clearly differentiate the biochemical changes. The loading plot illustrates distinctive peaks and

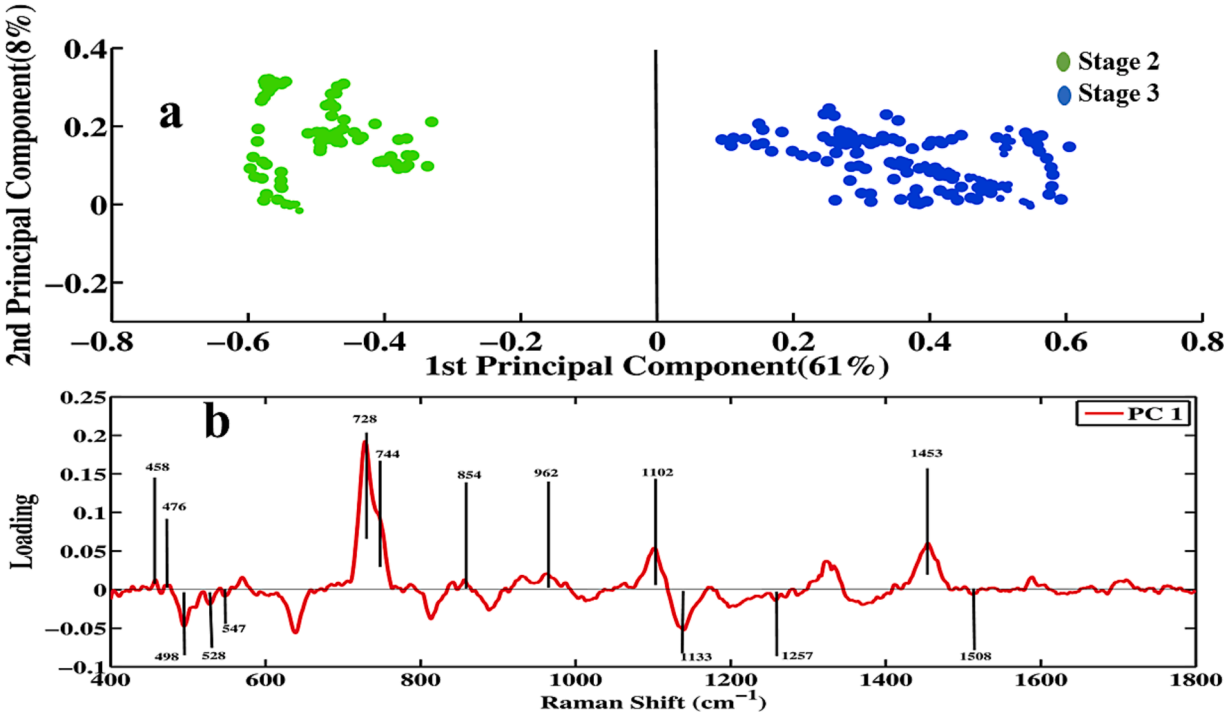


Fig. 4. Pairwise PCA scatter plot (a) and PCA loadings (b) of SERS spectral data sets of filtrate fraction of stage-2 versus stage-3.

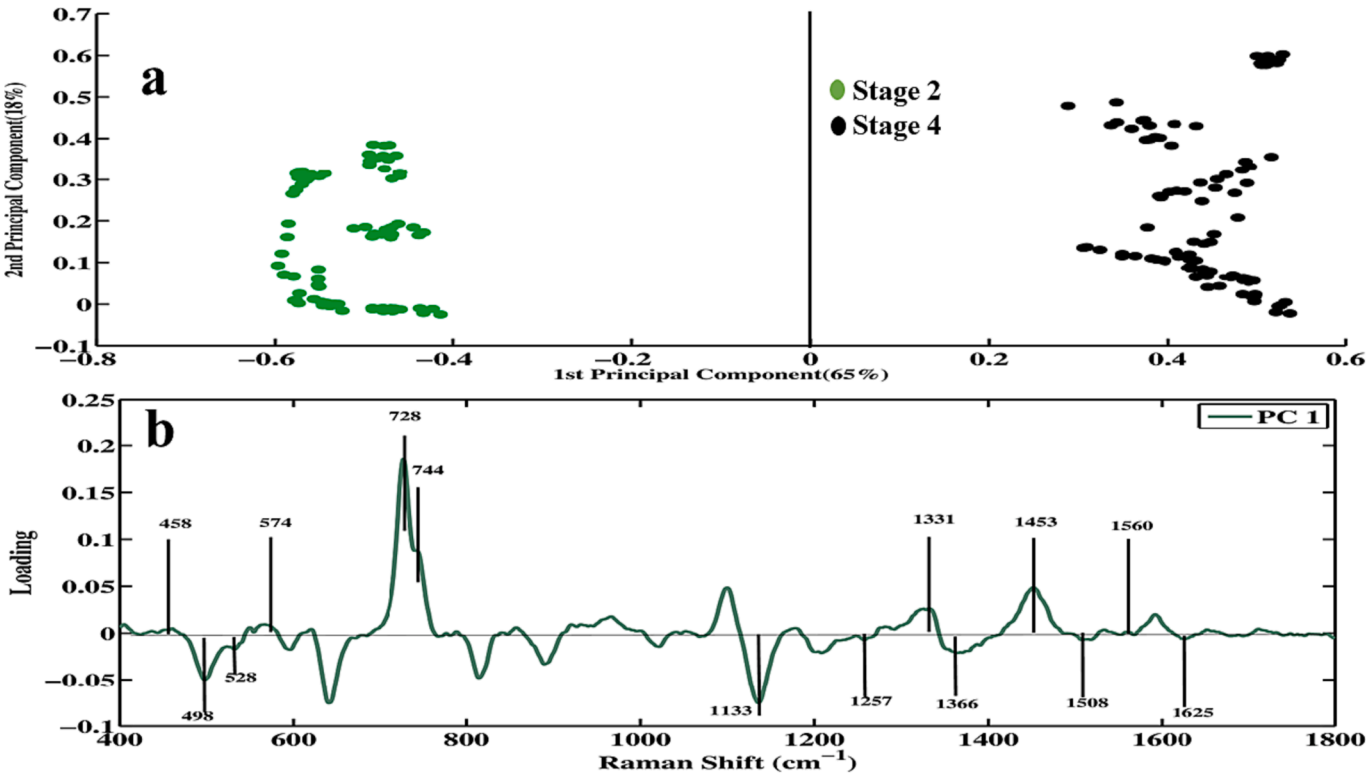


Fig. 5. Pairwise PCA scatter plot (a) and PCA loadings (b) of spectral data sets of filtrate fractions of stage 2 versus stage 4.

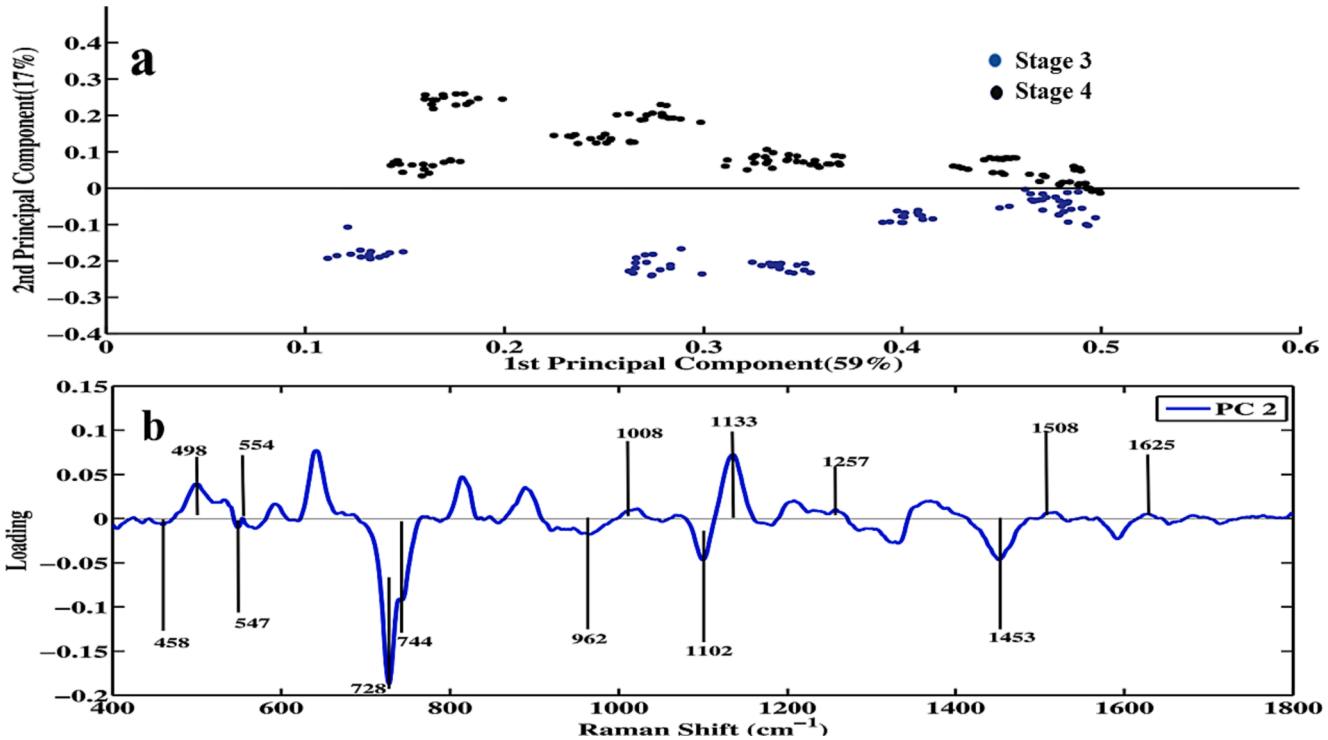


Fig. 6. (a) PCA scatter plot (a) and PCA loadings (b) of SERS spectral data sets of filtrate fraction of stage 3 and stage 4.

variations in intensities, highlighting differences. The non-cancerous samples associated with the peaks at negative loadings which are 574 cm^{-1} (tryptophan, protein), 728 cm^{-1} (adenine ring breathing mode, DNA), 744 cm^{-1} (thymine ring breathing mode), 784 cm^{-1} (O–P–O stretching), 1008 cm^{-1} (phenylaniline, protein), 1073 cm^{-1} (Triglycerides, fatty acids), 1133 cm^{-1} (palmitic acid), 1453 cm^{-1} (CH_2 bending, protein), 1588 cm^{-1} (C═CC Stretching mode) Adenine. The peaks appearing in positive loadings are related to cancerous samples which are 458 cm^{-1} (tryptophan), 476 cm^{-1} (glutamate, protein), 515 cm^{-1} (Phosphatidylinositol), 700 cm^{-1} (cholesterol, lipids), 864

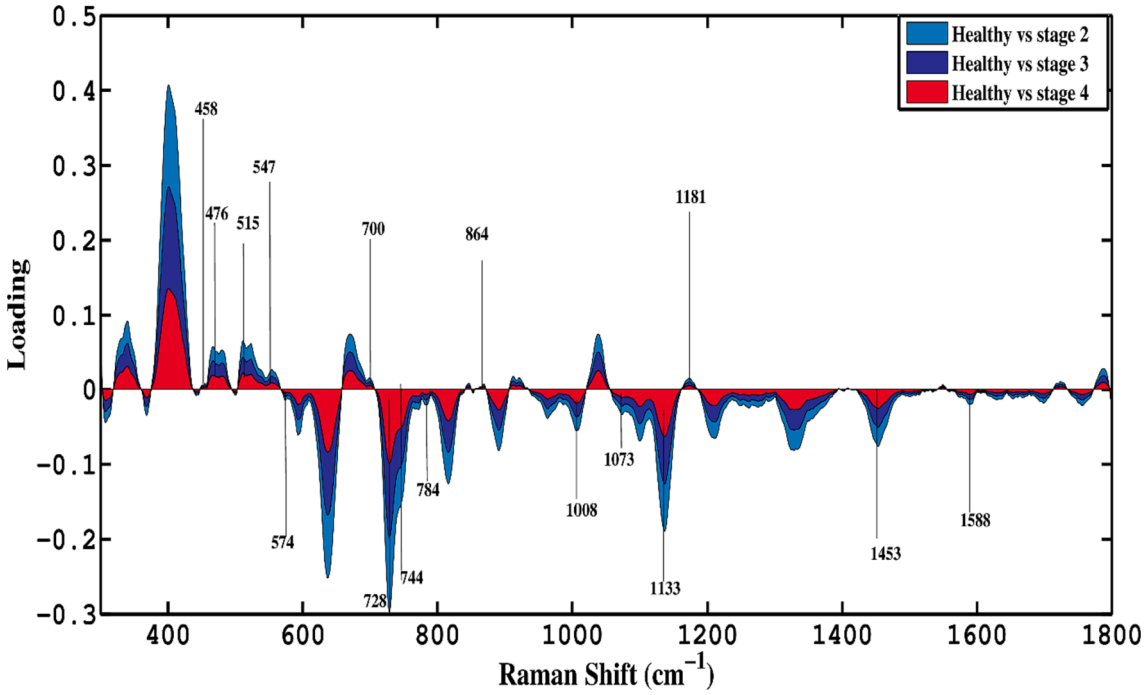


Fig. 7. PCA loadings of the SERS spectra of filtrate fractions of the blood serum samples of the healthy, stage2, stage3 and stage4 breast cancer stages.

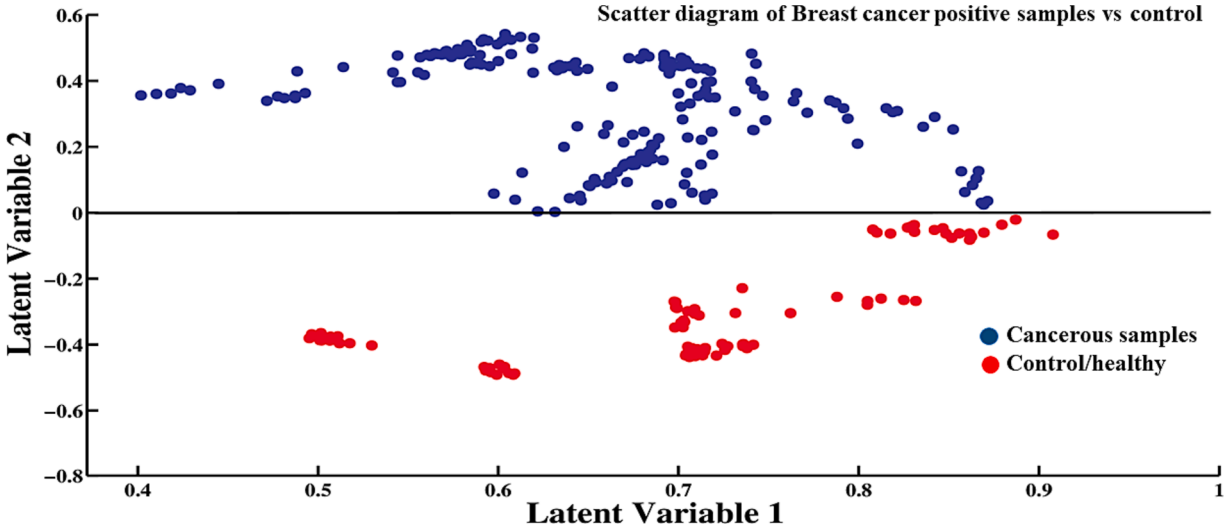


Fig. 8. Score plot illustrating the PLS-DA model for SERS spectra of filtrate fractions from both healthy and breast cancer serum samples of different stages.

cm^{-1} (C–H bond bending vibration) and 1181 cm^{-1} (C–H bending mode). These intensities clearly show the biochemical changes and disease biomarker features in different breast cancer stages.

3.4. Partial least square discriminant analysis

PLS-DA is a supervised chemometric approach that is used for differentiating the centrifugal filtrate of healthy control vs breast cancer stages have less than 30 kDa size. It's a data modelling approach that has been widely used in various fields like medical sciences and forensic [92]. In this study SERS spectral data was independently split in to two sets consisting of 40 % validation and 60 % calibration in order to eliminate biasedness in results, SERS spectral data was firstly put into matrix and then randomized. To reduce the overfitting of the data set and minimum number of latent variables were applied to build the model. Fig. 8 shows the score plot in the PLSDA model. The healthy filtrate samples (red color dots) were easily differentiated from filtrate of breast cancer stages filtrate (blue color dots) by using the PLSDA model. Fig. 9 shows the Receiver Operating Curve (ROC) of PLS-DA analysis of SERS spectral data sets of healthy control and disease samples and the AUC value obtained is 0.774. This model has the values 0—1 if the value is near to 1 then it clearly shows that the model was best fit and shows maximin 79 % accuracy, 76 % specificity and 81 % sensitivity. PLS-DA scatter score with all average spectra is presented in Fig. S7.

4. Conclusions

Surface-enhanced Raman spectroscopy, coupled with chemometrics, proves to be a highly valuable technique in this study. The use of centrifugal filtration devices reveals an improvement in the

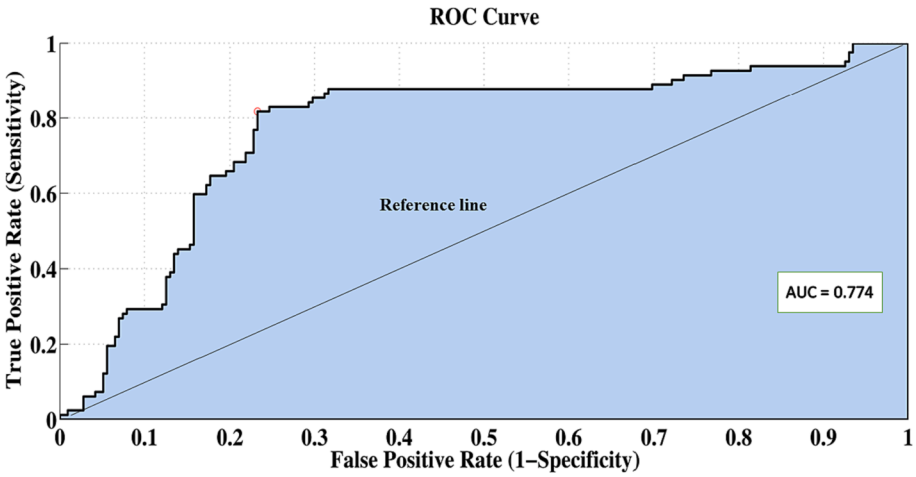


Fig. 9. Receiver operating curve (ROC) for the differentiation of SERS spectral data sets of filtrate fractions of healthy versus breast cancer samples of different stages.

characterization of SERS spectral features, particularly in the LMWF (Low Molecular Weight Fraction), which was previously overlooked, as the larger size biomolecules in HMWF (High Molecular Weight Fraction) dominate. The key differentiating SERS spectral features between the healthy control and different breast cancer stages appear at 839 cm^{-1}, 864 cm^{-1}, 970 cm^{-1}, 990 cm^{-1}, 1025 cm^{-1}, 1246 cm^{-1}, 1331 cm^{-1}, and 1673 cm^{-1}. SERS and statistical analysis hold promise as an efficient and reliable means for early detection and differentiation of breast cancer stages, offering valuable insights for potential clinical applications. PCA and PLS-DA were found helpful in the differentiation of breast cancer stages. The differentiation was done with 79 % accuracy, 76 % specificity and 81 % sensitivity.

CRediT authorship contribution statement

Hawa Hajab: Writing – original draft. **Ayesha Anwar:** Writing – review & editing. **Haq Nawaz:** Supervision. **Muhammad Irfan Majeed:** Project administration. **Najah Alwadie:** Resources. **Sana Shabbir:** Investigation. **Arooj Amber:** Methodology. **Muhammad Idrees Jilani:** Data curation. **Hafiza Faiza Nargis:** Visualization. **Muhammad Zohaib:** Validation. **Sidra Ismail:** Formal analysis. **Abida Kamal:** Software. **Muhammad Imran:** Resources.

Declaration of competing interest

The authors declare that they have no known competing financial interests or personal relationships that could have appeared to influence the work reported in this paper.

Data availability

Data will be made available on request.

Acknowledgments

The authors express their gratitude to Princess Nourah bint Abdulrahman University Researchers Supporting Project number (PNURSP2024R478), Princess Nourah bint Abdulrahman University, Riyadh, Saudi Arabia.

The authors express their appreciation to the Deanship of Scientific Research at King Khalid University, Saudi Arabia, for this work through research group program under grant number RGP-2/523/44.

Appendix A. Supplementary data

Supplementary data to this article can be found online at https://doi.org/10.1016/j.saa.2024.124046.

References

[1] J. Penders, et al., Single particle automated Raman trapping analysis of breast cancer cell-derived extracellular vesicles as cancer biomarkers, ACS Nano 15 (11) (2021) 18192–18205.
[2] Z. Cheng, et al., Application of serum SERS technology based on thermally annealed silver nanoparticle composite substrate in breast cancer, Photodiagn. Photodyn. Ther. 41 (2023) 103284.
[3] K. Polyak, Heterogeneity in breast cancer, J. Clin. Invest. 121 (10) (2011) 3786–3788.
[4] F. Wang, et al., Late-stage breast cancer diagnosis and health care access in Illinois, Prof. Geogr. 60 (1) (2008) 54–69.
[5] E. Vargas-Obieta, et al., Breast cancer detection based on serum sample surface enhanced Raman spectroscopy, Lasers Med. Sci. 31 (2016) 1317–1324.
[6] P. Caspers, et al., In vitro and in vivo Raman spectroscopy of human skin, Biospectroscopy 4 (S5) (1998) S31–S39.
[7] C. Krafft, et al., Near infrared Raman spectroscopic mapping of native brain tissue and intracranial tumors, Analyst 130 (7) (2005) 1070–1077.
[8] C.A. Lieber, et al., Raman microspectroscopy for skin cancer detection in vitro, J. Biomed. Opt. 13 (2) (2008), pp. 024013–024013-9.
[9] R. Karaballi, et al., Development of an electrochemical surface-enhanced Raman spectroscopy (EC-SERS) aptasensor for direct detection of DNA hybridization, PCCP 17 (33) (2015) 21356–21363.
[10] S.M. Hanash, C.S. Baik, O. Kallioniemi, Emerging molecular biomarkers—blood-based strategies to detect and monitor cancer, Nat. Rev. Clin. Oncol. 8 (3) (2011) 142–150.
[11] Y. Shen, et al., Characterization of the human blood plasma proteome, Proteomics 5 (15) (2005) 4034–4045.
[12] J.M. Jacobs, et al., Utilizing human blood plasma for proteomic biomarker discovery, J. Proteome Res. 4 (4) (2005) 1073–1085.
[13] N.L. Anderson, et al., The human plasma proteome: a nonredundant list developed by combination of four separate sources, Mol. Cell. Proteomics 3 (4) (2004) 311–326.
[14] A. Alpert, A. Shukla, Precipitation of large, high-abundance proteins from serum with organic solvents, The Association of Biomolecular Resource Facilities (ABRF), 2003(P111-W).
[15] J.M. Cameron, et al., Vibrational spectroscopic analysis and quantification of proteins in human blood plasma and serum, in: Vibrational Spectroscopy in Protein Research, Elsevier, 2020, pp. 269–314.
[16] H. Wennbo, J. TOÈrnell, The role of prolactin and growth hormone in breast cancer, Oncogene 19 (8) (2000) 1072–1076.
[17] G. Grieb, et al., Macrophage migration inhibitory factor (MIF): a promising biomarker, Drug News Perspect. 23 (4) (2010) 257.
[18] H. Zhang, et al., Role of gamma-synuclein in microtubule regulation, Exp. Cell Res. 317 (10) (2011) 1330–1339.
[19] L.-H. Gam, Breast cancer and protein biomarkers, World J. Exp. Med. 2 (5) (2012) 86.
[20] H. Pan, et al., Association between serum leptin levels and breast cancer risk: an updated systematic review and meta-analysis, Medicine 97 (27) (2018).
[21] D.W. Kufe, MUC1-C oncoprotein as a target in breast cancer: activation of signaling pathways and therapeutic approaches, Oncogene 32 (9) (2013) 1073–1081.

[22] F. Le Naour, et al., Identification of tumor-associated antigens using proteomics, Technol. Cancer Res. Treat. 1 (4) (2002) 257–262.
[23] R. Farese, et al., In vivo metabolic fingerprinting of neutral lipids with hyperspectral stimulated Raman scattering microscopy (2014).
[24] N. Gierlinger, M. Schwanninger, The potential of Raman microscopy and Raman imaging in plant research, J. Spectrosc. 21 (2007) 69–89.
[25] H.T. Ngo, et al., DNA bioassay-on-chip using SERS detection for dengue diagnosis, Analyst 139 (22) (2014) 5655–5659.
[26] M. Kashif, et al., Surface Enhanced Raman Spectroscopy of the serum samples for the diagnosis of Hepatitis C and prediction of the viral loads, Spectrochim. Acta A Mol. Biomol. Spectrosc. 242 (2020) 118729.
[27] S. Cervo, et al., SERS analysis of serum for detection of early and locally advanced breast cancer, Anal. Bioanal. Chem. 407 (2015) 7503–7509.
[28] A. Stefancu, et al., Combining SERS analysis of serum with PSA levels for improving the detection of prostate cancer, Nanomedicine 13 (19) (2018) 2455–2467.
[29] S. Bamrungsap, et al., SERS-fluorescence dual mode nanotags for cervical cancer detection using aptamers conjugated to gold-silver nanorods, Microchim. Acta 183 (2016) 249–256.
[30] R. Botta, et al., Tuberculosis determination using SERS and chemometric methods, Tuberculosis 108 (2018) 195–200.
[31] M.E. Hankus, D.N. Stratis-Cullum, P.M. Pellegrino, Characterization of next-generation commercial surface-enhanced Raman scattering (SERS) substrates, in: Chemical, Biological, Radiological, Nuclear, and Explosives (CBRNE) Sensing XII, 2011, SPIE.
[32] S. Preciado-Flores, et al., SERS spectroscopy and SERS imaging of Shewanella oneidensis using silver nanoparticles and nanowires, Chem. Commun. 47 (14) (2011) 4129–4131.
[33] M. Shakeel, et al., Surface-enhanced Raman spectroscopy for the characterization of pellets of biofilm forming bacterial strains of Staphylococcus epidermidis, Photodiagn. Photodyn. Ther. 40 (2022) 103145.
[34] S. Akbar, et al., Surface-Enhanced Raman Spectroscopic (SERS) characterization of low molecular weight fraction of the serum of breast cancer patients with principal component analysis (PCA) and partial least square-discriminant analysis (PLS-DA), Anal. Lett. 55 (10) (2022) 1588–1604.
[35] F. Bonnier, et al., Screening the low molecular weight fraction of human serum using ATR-IR spectroscopy, J. Biophotonics 9 (10) (2016) 1085–1097.
[36] H. Nawaz, et al., Evaluation of the potential of Raman microspectroscopy for prediction of chemotherapeutic response to cisplatin in lung adenocarcinoma, Analyst 135 (12) (2010) 3070–3076.
[37] H. Nawaz, et al., Prediction of viral loads for diagnosis of Hepatitis C infection in human plasma samples using Raman spectroscopy coupled with partial least squares regression analysis, J. Raman Spectrosc. 48 (5) (2017) 697–704.
[38] I.T. Jolliffe, Principal Component Analysis for Special Types of Data, Springer, 2002.
[39] F. Westad, F. Marini, Validation of chemometric models–a tutorial, Anal. Chim. Acta 893 (2015) 14–24.
[40] T. Zelmanovitz, et al., The receiver operating characteristics curve in the evaluation of a random urine specimen as a screening test for diabetic nephropathy, Diabetes Care 20 (4) (1997) 516–519.
[41] M. Librán-Pérez, et al., Antiviral activity of palmitic acid via autophagic flux inhibition in zebrafish (Danio rerio), Fish Shellfish Immunol. 95 (2019) 595–605.
[42] J. Mayneris-Perxachs, et al., Plasma fatty acid composition, estimated desaturase activities, and their relation with the metabolic syndrome in a population at high risk of cardiovascular disease, Clin. Nutr. 33 (1) (2014) 90–97.
[43] Y.-H. Hsiao, et al., Palmitic acid-induced neuron cell cycle G2/M arrest and endoplasmic reticular stress through protein palmitoylation in SH-SY5Y human neuroblastoma cells, Int. J. Mol. Sci. 15 (11) (2014) 20876–20899.
[44] X. Wang, C. Zhang, N. Bao, Molecular mechanism of palmitic acid and its derivatives in tumor progression, Front. Oncol. 13 (2023) 1224125.
[45] J.S. Soares, et al., Diagnostic power of diffuse reflectance spectroscopy for targeted detection of breast lesions with microcalcifications, Proc. Natl. Acad. Sci. 110 (2) (2013) 471–476.
[46] Y. Mei, et al., Plasma fibrinogen level may be a possible marker for the clinical response and prognosis of patients with breast cancer receiving neoadjuvant chemotherapy, Tumor Biol. 39 (6) (2017), 1010428317700002.
[47] J. De Gelder, et al., Reference database of Raman spectra of biological molecules, J. Raman Spectrosc. 38 (9) (2007) 1133–1147.
[48] M. Akram, et al., Surface-enhanced Raman spectroscopy for characterization of filtrate portions of blood serum samples of typhoid patients, Photodiagn. Photodyn. Ther. 40 (2022) 103199.
[49] D. Chalapathi, et al., Surface-enhanced Raman spectroscopy as a tool for distinguishing extracellular vesicles under autophagic conditions: a marker for disease diagnostics, J. Phys. Chem. B 124 (48) (2020) 10952–10960.
[50] C. Krafft, et al., Near infrared Raman spectra of human brain lipids, Spectrochim. Acta A Mol. Biomol. Spectrosc. 61 (7) (2005) 1529–1535.
[51] Y. Liu, et al., Label and label-free based surface-enhanced Raman scattering for pathogen bacteria detection: a review, Biosens. Bioelectron. 94 (2017) 131–140.
[52] Z. Movasaghi, S. Rehman, I.U. Rehman, Raman spectroscopy of biological tissues, Appl. Spectrosc. Rev. 42 (5) (2007) 493–541.
[53] H. Nargis, et al., Comparison of surface enhanced Raman spectroscopy and Raman spectroscopy for the detection of breast cancer based on serum samples, Spectrochim. Acta A Mol. Biomol. Spectrosc. 246 (2021) 119034.
[54] C.J. Frank, R.L. McCreery, D.C. Redd, Raman spectroscopy of normal and diseased human breast tissues, Anal. Chem. 67 (5) (1995) 777–783.
[55] S. Farquharson, et al., Analysis of 5-fluorouracil in saliva using surface-enhanced Raman spectroscopy, J. Raman Spectrosc. 36 (3) (2005) 208–212.
[56] R. Haldavnekar, K. Venkatakrishnan, B. Tan, Cancer stem cell derived extracellular vesicles with self-functionalized 3D nanosensor for real-time cancer diagnosis: eliminating the roadblocks in liquid biopsy, ACS Nano 16 (8) (2022) 12226–12243.
[57] N. Kuhar, et al., Challenges in application of Raman spectroscopy to biology and materials, RSC Adv. 8 (46) (2018) 25888–25908.
[58] W.T. Cheng, et al., Micro-Raman spectroscopy used to identify and grade human skin pilomatrixoma, Microsc. Res. Tech. 68 (2) (2005) 75–79.
[59] Y. Wang, et al., Photocatalytically powered matchlike nanomotor for light-guided active SERS sensing, Angew. Chem. 130 (40) (2018) 13294–13297.
[60] Z. Huang, et al., Near-infrared Raman spectroscopy for optical diagnosis of lung cancer, Int. J. Cancer 107 (6) (2003) 1047–1052.
[61] P. Raja, et al., Characterization of blood plasma of normal and cervical cancer patients using NIR Raman spectroscopy, Vib. Spectrosc 102 (2019) 1–7.
[62] R.C. Tomas, et al., Detection of breast cancer by ATR-FTIR spectroscopy using artificial neural networks, PLoS One 17 (1) (2022) e0262489.
[63] A. Blat, et al., Fourier transform infrared spectroscopic signature of blood plasma in the progression of breast cancer with simultaneous metastasis to lungs, J. Biophotonics 12 (10) (2019) e201900067.
[64] R. Haldavnekar, et al., Prediction of cancer stem cell fate by surface-enhanced Raman scattering functionalized nanoprobes, ACS Nano 14 (11) (2020) 15468–15491.
[65] M. Gniadecka, et al., Diagnosis of basal cell carcinoma by Raman spectroscopy, J. Raman Spectrosc. 28 (2–3) (1997) 125–129.
[66] S. Bashir, et al., Surface-enhanced Raman spectroscopy for the identification of tigecycline-resistant E. coli strains, Spectrochim. Acta A Mol. Biomol. Spectrosc. 258 (2021) 119831.
[67] E. Efeoglu, M. Culha, In situ-monitoring of biofilm formation by using surface-enhanced Raman scattering, Appl. Spectrosc. 67 (5) (2013) 498–505.
[68] L. Silveira Jr, et al., Correlation between near-infrared Raman spectroscopy and the histopathological analysis of atherosclerosis in human coronary arteries, Lasers Surg. Med. 30 (4) (2002) 290–297.
[69] E. Gavgiotaki, et al., Detection of the T cell activation state using nonlinear optical microscopy, J. Biophotonics 12 (3) (2019) e201800277.
[70] I. Rehman, Z. Movasaghi, S. Rehman, Vibrational Spectroscopy for Tissue Analysis, Taylor & Francis, 2012.
[71] J. Depciuch, et al., The spectroscopic similarity between breast cancer tissues and lymph nodes obtained from patients with and without recurrence: a preliminary study, Molecules 25 (14) (2020) 3295.
[72] S. Aghamiri, A. Jafarpour, M. Shoja, Retracted: Effects of silver nanoparticles coated with anti-HER2 on irradiation efficiency of SKBR3 breast cancer cells, IET Nanobiotechnol. 13 (8) (2019) 808–815.
[73] R.K. Dukor, Vibrational spectroscopy in the detection of cancer, Handbook of Vibrational Spectroscopy (2006).
[74] Z. Huang, et al., Raman spectroscopy in combination with background near-infrared autofluorescence enhances the in vivo assessment of malignant tissues, Photochem. Photobiol. 81 (5) (2005) 1219–1226.
[75] G.F. Ştiufiuc, et al., Solid plasmonic substrates for breast cancer detection by means of SERS analysis of blood plasma, Nanomaterials 10 (6) (2020) 1212.
[76] V.C. Munteanu, et al., New insights into the multivariate analysis of SER spectra collected on blood samples for prostate cancer detection: towards a better understanding of the role played by different biomolecules on cancer screening: a preliminary study, Cancers 14 (13) (2022) 3227.
[77] R. Malini, et al., Discrimination of normal, inflammatory, premalignant, and malignant oral tissue: a Raman spectroscopy study, Biopolymers: Original Res. Biomol. 81 (3) (2006) 179–193.
[78] G. Shetty, et al., Raman spectroscopy: elucidation of biochemical changes in carcinogenesis of oesophagus, Br. J. Cancer 94 (10) (2006) 1460–1464.
[79] C.-H. Liu, et al., Resonance Raman and Raman spectroscopy for breast cancer detection, Technol. Cancer Res. Treat. 12 (4) (2013) 371–382.
[80] X. Wang, et al., Novel SERS biosensor for rapid detection of breast cancer based on Ag2O-Ag-PSi nanochips, Spectrochim. Acta Part A (2023) 123226.
[81] C.L. Morais, F.S. Costa, K.M. Lima, Variable selection with a support vector machine for discriminating Cryptococcus fungal species based on ATR-FTIR spectroscopy, Anal. Methods 9 (20) (2017) 2964–2970.
[82] D. Mabwa, et al., Mid-infrared spectral classification of endometrial cancer compared to benign controls in serum or plasma samples, Analyst 146 (18) (2021) 5631–5642.
[83] A.H. Nguyen, E.A. Peters, Z.D. Schultz, Bioanalytical applications of surface-enhanced Raman spectroscopy: de novo molecular identification, Rev. Anal. Chem 36 (4) (2017) 20160037.
[84] C.P. Marshall, A. Olcott Marshall, The potential of Raman spectroscopy for the analysis of diagenetically transformed carotenoids, Philos. Trans. R. Soc. A Math. Phys. Eng. Sci. 2010 (368) (1922) 3137–3144.

[85] T. Bhattacharjee, et al., Swiss bare mice: a suitable model for transcutaneous in vivo Raman spectroscopic studies of breast cancer, Lasers Med. Sci. 29 (2014) 325–333.
[86] R.J. Lakshmi, et al., Tissue Raman spectroscopy for the study of radiation damage: brain irradiation of mice, Radiat. Res. 157 (2) (2002) 175–182.
[87] S. Ahmad, et al., Characterization and prediction of viral loads of Hepatitis B serum samples by using surface-enhanced Raman spectroscopy (SERS), Photodiagn. Photodyn. Ther. 35 (2021) 102386.
[88] V. Balan, et al., Vibrational spectroscopy fingerprinting in medicine: from molecular to clinical practice, Materials 12 (18) (2019) 2884.
[89] G. Cennamo, et al., Surface-enhanced Raman spectroscopy of tears: toward a diagnostic tool for neurodegenerative disease identification, J. Biomed. Opt. 25 (8) (2020) 087002.
[90] F.M.V. Meza, Characterization of Mexican Breast Cancer Cells by Raman Microspectroscopy and Atomic Force Microscopy.
[91] X. Cao, et al., Label-free detection of human serum using surface-enhanced Raman spectroscopy based on highly branched gold nanoparticle substrates for discrimination of non-small cell lung cancer, J. Chem. 2018 (2018) 1–13.
[92] G. Dastgir, et al., Surface-enhanced Raman spectroscopy of polymerase chain reaction (PCR) products of Rifampin resistant and susceptible tuberculosis patients, Photodiagn. Photodyn. Ther. 38 (2022) 102758.